Dalton Transactions

Accepted Manuscript

ROYAL SOCIETY OF CHEMISTRY

www.rsc.org/dalton

Construction of $Cu_3Mo_2O_9$ Nanoplates with Excellent Lithium Storage Properties Based on a pH-Dependent Dimensional Change†

Juan Xia[a], Le Xin Song*[a,b], Wei Liu*[a], Yue Teng[a], Li Zhao[b], Qing Shan Wang[b] and Mao Mao Ruan[b]

Received 1st May 2015, Accepted Xth XXXXXXXXX 2015
First published on the web Xth XXXXXXXXX 2015
DOI: 10.1039/b000000h

One-, two- and three-dimensional nanostructures of copper molybdenum oxide hydroxide were successfully constructed by a simple approach through a pH-dependent dimensional transformation of ammonium copper molybdate. Thin nanoplates of copper molybdate, which were obtained by sintering the two-dimensional nanobelts of copper molybdenum oxide hydroxide, exhibited remarkably high reversible lithium storage capacity, good rate capability and excellent cycling stability.

Molybdenum oxides have been extensively used as anode materials in lithium-ion batteries (LIBs),[1–3] due to their unique physical and electrochemical properties. However, only a few studies have characterized the application of transition metal molybdates in LIBs.[4,5] Further, most of the reported cases showed a relatively low reversible capacity than molybdenum oxides.[6,7] For example, the 2D $CoMoO_4$ nanoplates and 3D $Co_2Mo_3O_8$ submicron particles possessed reversible capacities of 560 mAh·g^{-1} after 50 cycles[8] and 425 mAh·g^{-1} after 40 cycles,[9] respectively. Also, we noticed that the highly monodisperse 3D copper molybdate ($Cu_3Mo_2O_9$, CM) micropompons only exhibited a reversible capacity of 129 mAh·g^{-1} after 60 cycles, even though they can maintain excellent charge-discharge stability and very high coulombic efficiency during 100 charge-discharge cycles.[10] It constitutes a challenge: how to improve the reversible capacity of transition metal molybdates.

Our essential idea is to understand the influence of structure of CM (a typical transition metal molybdate), specifically dimensional changes, on LIBs performance. Therefore, in the framework of the present study, we developed a method to synthesize different dimensional nanostructured CM materials by an efficient and reliable technique. Initially, we prepared ammonium copper molybdate [$(NH_4)_2Cu(MoO_4)_2$, ACM-**1**] using the reaction of ammonium molybdate tetrahydrate (AMT, 0.72 mmol) with copper acetate dihydrate (CAD, 2.50 mmol) at 383 K for 30 min under hydrothermal conditions (Experimental section, ESI†). Subsequently, a series of copper molybdenum oxide hydroxide [$Cu_3(OH)_2(MoO_4)_2$, CMOH] materials with various dimensions, including 1D, 2D and 3D nanostructures, as the precursor of CM were obtained through a pH-dependent dimensional transformation of the ACM-**1** (Figure 1). Finally, the CMOHs were sintered at 773 K for 3 h in a muffle furnace to produce CMs, in which the shapes of the CMOHs can be maintained. To the best of our knowledge, this is the first example of pH-induced dimensional transformation of molybdates. More importantly, we found that the structure of CM, especially dimensional changes, significantly affects the reversible capacity of LIBs. For example, 2D nanoplates showed much higher levels than 1D and 3D structures. We believe that this work represents an important advance regarding molybdate materials.

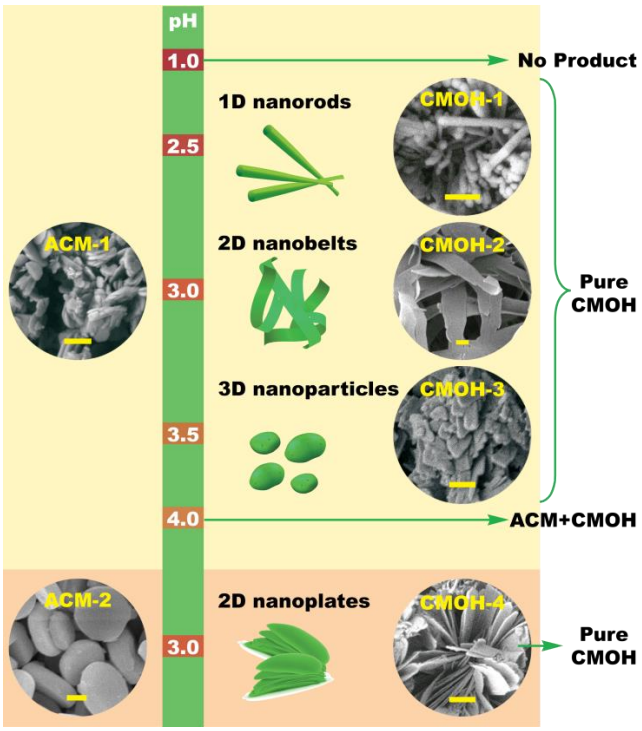

Figure 1. Schematic illustration describing the formation of the CMOHs with different dimensions derived from ACMs at initial pH values of 2.0, 2.5 and 3.0. Scale bars are 1 μm for ACMs and 500 nm for CMOHs.

As seen from field-emission scanning electron microscopy images (FE-SEM, Figure 1), three kinds of CMOHs with different dimensions, namely 1D nanorods (CMOH-**1**), 2D nanobelts (CMOH-**2**) and 3D nanoparticles (CMOH-**3**), were successfully fabricated in high yields (79, 93 and 88%, respectively) using a pH-driven procedure from irregular particles of the ACM-**1** (Figure 1 and Figure S1, ESI†; diameter, 0.5~1.5 μm) to the CMOHs (Equation 1). The crystallographic structure and phase purity of the CMOHs were determined by X-ray diffraction (Figure S2, ESI†). All of the diffraction peaks were assigned to a monoclinic structure with a space group of $P2_1/n$ (JCPDS 86−2311).[11] No impurity was found. As shown in Figure 1, the

[a]*CAS Key Laboratory of Materials for Energy Conversion & Collaborative Innovation Center of Suzhou Nano Science and Technology, Department of Materials Science and Engineering, University of Science and Technology of China, Jinzhai Road 96, Hefei, China 230026;*
[b]*Department of Chemistry, University of Science and Technology of China, Jinzhai Road 96, Hefei, China 230026;*
E-mail: solexin@ustc.edu.cn; wliu@ustc.edu.cn;

†Electronic supplementary information (ESI) available: Preparation, Instruments, XRD patterns, BET, EDS, WDXRF, XPS profiles, See DOI: 10.1039/b000000h.

CMOH-**1** nanorods (diameter, 150 nm; length, 2~3 μm), CMOH-**2** nanobelts (thickness, 100 nm; width, 1~2 μm; length, 5~7 μm) and CMOH-**3** nanoparticles (diameter, 100~400 nm) were obtained at initial pH values of 2.0, 2.5 and 3.0, respectively. This result strongly suggests that a pH-dependent dimensional change occurred in the process from the ACM-**1** to the CMOHs.

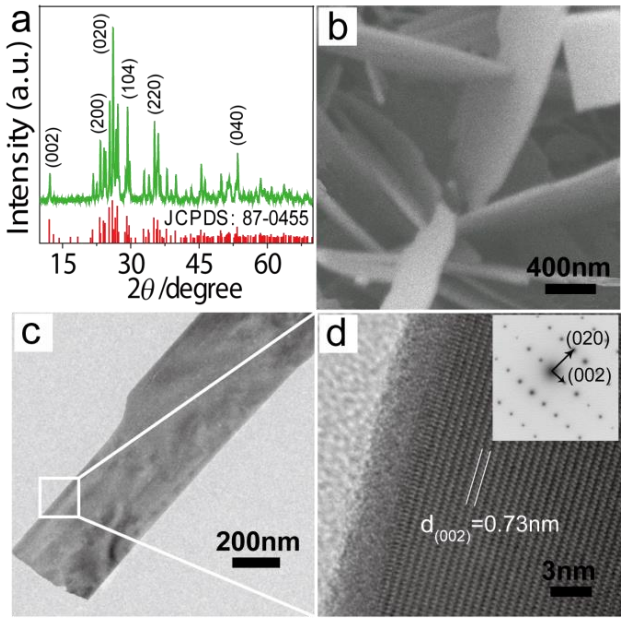

Figure 2. XRD pattern (a) and FE-SEM image (b) of CM-**2** nanoplates; TEM micrograph (c) and HR-TEM image (d) of a single CM-**2** nanoplate; the inset in Figure 2d shows the SAED pattern of a single CM-**2** nanoplate.

$$\text{ACM} + H^+ \longrightarrow \underbrace{Cu^{2+} + MoO_4^{2-}}_{\text{CMOH}} \quad 1)$$

$$\text{CMOH} \longrightarrow \text{CM} + H_2O \quad 2)$$

We noticed that the ACM-**1** can be sufficiently dissolved in HCl to produce Cu^{2+} and MoO_4^{2-} ions in the pH range of 2.5~3.5. Therefore, the pH-driven procedure may be regarded as a dissolution-precipitation process with different levels of details. Further, we found that the ACM-**1** cannot be fully dissolved at lower acidity (eg, pH=4 and 5, Figure S3, ESI†), while higher acidity led to the complete dissolution of the CMOH (eg, pH=1, Figure S4, ESI†). This result is interesting because it allows us to consider that the acidity plays an important role in creating the structures of the CMOHs. Clearly, the effect of acidity is associated with relative growth rate of crystal directions, since relatively higher acidity is favourable for the 1D growth, moderate acidity for the 2D growth and relatively lower acidity for the 3D growth. We think that the precipitation transformation and especially the dimensional transition driven by pH gradients are very important to the evolution and development of later inorganic nanomaterials.

Also, we obtained a 2D nanoplate material of CMOH-**4** (thickness, 100 nm; width, 500 nm; length, 4~5 μm) at an initial pH of 3.0 based on the same dissolution-precipitation process using the disc-like ACM-**2** (diameter, 1.5~3 μm; thickness, 300~600 nm, Figure 1 and Figure S1, ESI†) as precursor. This means that the structure of ACMs is not related to the crystal-forming process of CMOHs.

Moreover, the CM-**1** (1D nanorods), CM-**2** (2D nanoplates, Figure 2) and CM-**3** (3D nanoparticles) were successfully synthesized (Equation 2, Figure S5, ESI†) by simply sintering the CMOH-**1**, CMOH-**2** and CMOH-**3** at 773 K for 3 h, respectively. As seen in Figure 2a, all of the reflection peaks of the CM-**2** can be readily indexed as a pure orthorhombic structure with a space group of Pnma (JCPDS 87−0455).[12] No impurity diffraction peak was detected. In addition, the diffraction peaks were quite narrow, indicating high crystallinity.

The X-ray energy dispersive spectrometry (EDS, Figure S6, ESI†) analysis confirms that the CM-2 contains only elements of Cu, Mo and O, and the molar ratio of Cu:Mo:O is approximately 3:2:9. Further, the wavelength-dispersive X-ray fluorescence spectrometry (WDXRF, Figure S7, ESI†) analysis indicates that the weight contents (wt%) of Cu and Mo elements in the CM-2 material are 36.19 and 36.35% respectively, which provides additional evidence for the EDS results. It is worth stressing that the CM-2 nanoplates show fairly smooth surfaces (Figure 2b) and are very thin, with a thickness of smaller than 50 nm. The transmission electron microscopy (TEM, Figure 2c) image of a single nanoplate reveals that the width is about 300 to 400 nm. By comparing the structures of the CMOH-**2** and CM-**2**, we can roughly infer that the thermal decomposition reaction from the precursor to the final product can result in a morphology change from nanobelts to nanoplates, but does not cause a change in dimension. High-resolution TEM (HR-TEM, Figure 2d) indicates that the CM-**2** nanoplate is single crystalline with a spacing of 0.73 nm corresponding to (002) planes. The selected area electron diffraction (SAED) pattern in the inset of Figure 2d shows that the nanoplate crystal has an ordered lattice structure and the diffraction spots are well consistent with the (002) and (020) planes of the orthorhombic CM phase. From the X-ray photoelectron spectroscopy (XPS) survey spectrum (Figure S8, ESI†) of the CM-**2** nanoplates, only Cu, Mo and O are observable, and the binding energies of Cu(II) and Mo(VI) are the same as those reported in the previous study.[13]

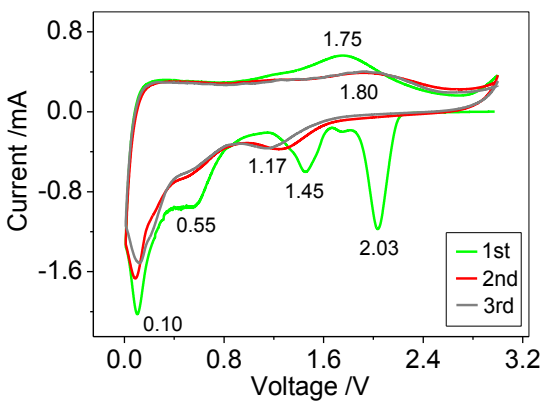

Figure 3. The first three consecutive CV scans of the electrodes made from the CM-**2** nanoplates at a scan rate of 0.2 $mV \cdot s^{-1}$ in the voltage range 0.01~3.00 V versus Li^+/Li.

Further, we investigate the electrochemical property of the CM-**2** by cyclic voltammetry (CV). Figure 3 illustrates the CV curves of the CM nanoplates at a scan rate of 0.20 $mV \cdot s^{-1}$ in the potential range of 0.01~3.00 V. Obviously, the curve of the first cycle is different from those for the following cycles, and no significant change was seen between the second and third cycles, suggesting a electrochemical behaviour similar to other metal oxides in LIBs.[14]

$$Cu_3Mo_2O_9 + 18Li \longrightarrow 3Cu + 2Mo + 9Li_2O \quad 3)$$

$$Mo + 2Li_2O \rightleftharpoons MoO_2 + 4Li \quad 4)$$

$$MoO_2 + Li_2O \rightleftharpoons MoO_3 + 2Li \quad 5)$$

In the first cathodic sweep, the peaks at 2.03 and 1.45 V are attributed to the intercalation of lithium ions into the CM lattice, forming the stable intermediate Li_xMoO_3.[15] The other two can be regarded as the reductions of Cu(II) to Cu(0) at 0.55 V and Mo(IV) to Mo(0) at 0.10 V (Equation 3).[16,17]

The broad oxidation peak at about 1.75 V in the anodic scan corresponds to the oxidation of Mo(0) to Mo(IV) (Equation 4).[15b] Besides, in the second and third cycles, it is observed that a new cathodic peak occurs at 1.17 V, owing to the reduction of Cu(II) to Cu(I).[18] The broader oxidation peak at 1.80 V is ascribed to partial oxidation of Mo(IV) to Mo(VI) (Equation 5).[9] The positive shift of the anodic peak may be due to the polarization phenomenon of the electrodes in the first cycle.[19]

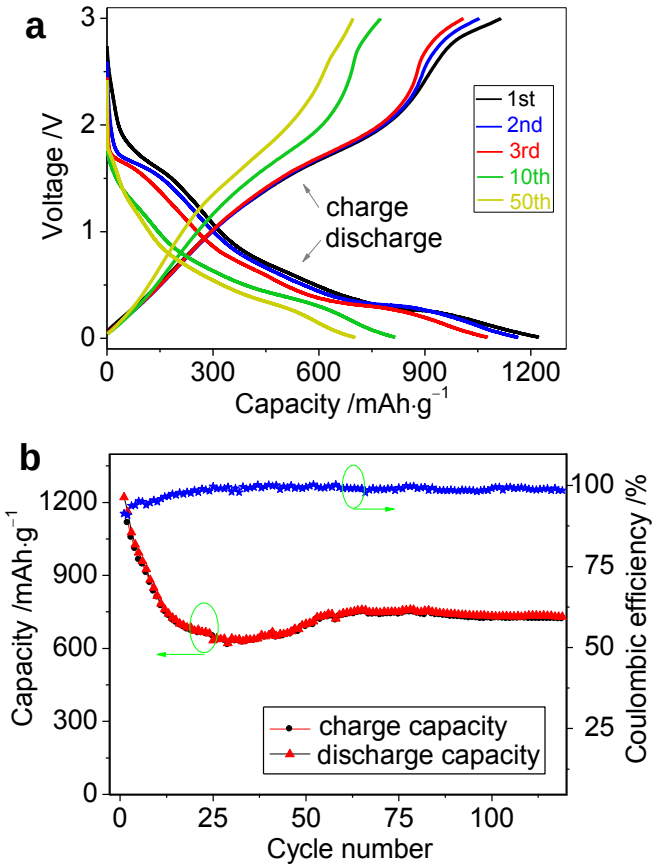

Figure 4. (a) Charge-discharge voltage profiles of the CM-**2** electrode at the first, second, third, tenth and fiftieth cycles and (b) cycling performance and coulombic efficiency of the electrode at a current density of 100 mA·g^{-1}.

According to the CV results, the lithium storage mechanism of the CM-**2** is mainly associated with the formation of the irreversible Li–Cu–O and the electrochemically active Li_xMoO_y during the charge and discharge process.[20]

Figure 4a displays the charge-discharge curves of the CM-**2** nanoplates in the voltage range from 0.01 to 3.00 V at a constant current density of 100 mA·g^{-1}. At first, second, and third cycles, the discharge and charge capacities of the electrode material are 1225, 1163 and 1079 mAh·g^{-1}, and 1123, 1057 and 1059 mAh·g^{-1}, respectively. The low irreversible capacity loss of around 8.3% at this constant current density may be ascribed to the occurrence of irreversible processes, such as the formation of solid–electrolyte interface layer and the trapping of some lithium in the lattice of the electrode material.[21,22] After 10 and 50 cycles, the CM-**2** electrode exhibits the discharge capacities of 823 and 720 mAh·g^{-1} at a constant current density of 100 mA·g^{-1}, as seen from this figure.

Figure 4b presents the cycle performance and coulombic efficiency of the CM-**2** nanoplates at a current density of 100 mA·g^{-1}. The specific capacity first decreases slowly (from cycle 1 to cycle 13), then increases and finally levels off (from cycle 14 to cycle 120). Such a change in capacity, which is somewhat similar to, but not the same as that observed for some alloys of transition metals in LIBs, may be due to the electrochemical activation of the electrode material.[23] It is worthy of note that even after 120 cycles the reversible capacity of the electrode is still up to 746 mAh·g^{-1}, which is about six times greater than that of the CM microspheres.[10]

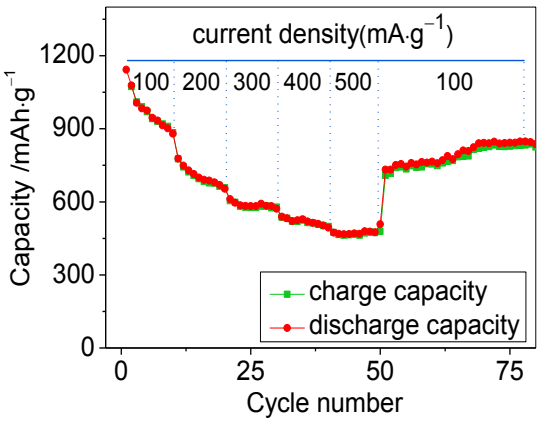

Figure 5. The rate performance of the CM-**2** electrode at the current densities of 100, 200, 300, 400 and 500 mA·g^{-1}.

The coulombic efficiency of the CM-**2** nanoplates is about 90% during the first few cycles, and remains above 99% in the subsequent cycles until the 120th cycle. It suggests the coulombic stability in the reversible formation and decomposition process of the Li_xMoO_y phase. Such an increase in coulombic efficiency is of great importance since an electrode with an increased coulombic efficiency will consume less fuel to gain more energy.

The rate performance of the CM-**2** material was shown in Figure 5. The average capacities were determined to be 940, 682, 608, 537 and 484 mAh·g^{-1} at the current densities of 100, 200, 300, 400 and 500 mA·g^{-1}, respectively. As far as we know, this is one of the only two examples for the rate comparison of transition metal molybdates in LIBs.[24] Although the capacities were gradually decreased with the increase of current densities, it is striking that this material still retains a reversible capacity of 484 mAh·g^{-1} even at a current density of 500 mA·g^{-1}, exhibiting excellent rate capability. In particular, after being tested at high rates, the material still can be partially recovered since it presents an increasing capacity at a current density of 100 mA·g^{-1}, which implies that the structure of the electrode is considerably stable. To our knowledge, our results represent the highest efficiency reported to date for any transition metal molybdates in LIBs under standard conditions (Table 1, ESI†).[5c,8,9,20,24,25]

In addition, the electrochemical performance of the CM-**1** nanorods and CM-**3** nanoparticles were investigated in comparison with that of the CM-**2** nanoplates. We found that the nanorod and nanoparticle electrodes exhibit much lower charge-discharge capacities (301 mAh·g^{-1} and 208 mAh·g^{-1}, Figure S9, ESI†) after 120 cycles than the nanoplate electrode at a current density of 100 mA·g^{-1}.

To understand the high capacity and good cyclability of the

CM-**2** electrode, we examined the surface characteristics of these materials by nitrogen adsorption-desorption isotherms (Figure S10, ESI†). Our data indicate that the Brunauer-Emmett-Teller (BET)[26] specific surface areas and Barrett–Joyner–Halenda (BJH)[27] pore diameters of the 1D nanorods, 2D nanoplates and 3D nanoparticles are 4.5 $m^2 \cdot g^{-1}$ and 71 nm, 19.4 $m^2 \cdot g^{-1}$ and 30 nm, and 3.4 $m^2 \cdot g^{-1}$ and 44 nm, respectively. It is clear that the nanoplate electrode presents a much higher BET surface area and a much lower BJH pore diameter than the nanorod and nanoparticle electrodes. The difference in surface structure can be an important reason why the materials performed different electrochemical behaviours in LIBs. The nanoplate structure with a larger BET surface and a smaller pore diameter may possess more exposed active sites and interfaces. On the other hand, the thin 2D plate nanostructure also can significantly shorten the diffusion distance of Li ions and thus facilitates the lithium insertion-extraction kinetics.[28,29]

In summary, in the present paper we report on a new possibility of a controlled structural transition from ACM to CMOH by changing pH in water. To our knowledge, this is the first paradigm showing that a dissolution/precipitation equilibrium between the two transition metal molybdates may be accompanied by a dimensional transformation between them in a pH-driven process. A series of CMOH nanomaterials with different dimensions (from 1D nanorods, 2D nanobelts, to 3D nanoparticles) were successfully constructed using this equilibrium model. Moreover, there were no significant structural and dimensional changes as a result of the transformation procedure from CMOH to CM. Further, two nanomaterials: CM-**1** nanorods and CM-**2** nanoplates were obtained through this transformation process and evaluated with respect to their possible application in LIBs. Our data provided strong evidence that the CM-**2** nanoplates exhibited greatly enhanced lithium storage properties, including very high storage capacity, extremely high coulombic efficiency and excellent cycling stability, compared to the other structures such us nanorods, microflowers and so on. It can be attributed to ultrafine particle size, very thin planar structure and large surface area. We think that the present study provides a starting point for further research on the controlled synthesis of inorganic nanomaterials using a pH-driven precipitation equilibrium transition, and believe that the as-obtained CM-**2** is a potential anode material for LIBs due to its efficient and environmental friendly synthesis.

Acknowledgments

This project was supported by NSFC (No. 21071139) and Natural Science Foundation of Anhui Province (No. 1508085MB30).

References

1 a) Y. M. Sun, X. L. Hu, J. C. Yu, Q. Li, W. Luo, L. X. Yuan, W. X. Zhang, Y. H. Huang, *Energ. Environ. Sci.*, 2011, **4**, 2870. b) X. F. Zhang, X. X. Song, S. Gao, Y. M. Xu, X. L. Cheng, H. Zhao, L. H. Huo, *J. Mater. Chem. A*, 2013, **1**, 6858. c) J. S. Chen, Y. L. Cheah, S. Madhavi, X. W. Lou, *J. Phys. Chem. C*, 2010, **114**, 8675.

2 a) Q. Wang, J. Sun, Q. Wang, D. A. Zhang, L. L. Xing, X. Y. Xue, *J. Mater. Chem. A*, 2015, **3**, 5083. b) U. K. Sen, A. Shaligram, S. Mitra, *Acs. Appl. Mater. Inter.*, 2014, **6**, 14311.

3 a) Z. Y. Wang, J. S. Chen, T. Zhu, S. Madhavi, X. W. Lou, *Chem. Commun.*, 2010, **46**, 6906. b) H. J. Zhang, J. Shu, K. X. Wang, X. T. Chen, Y. M. Jiang, X. Wei, J. S. Chen, *J. Mater. Chem. A*, 2014, **2**, 80.

4 a) Y. Ding, Y. Wan, Y. L. Min, W. Zhang, S. H. Yu, *Inorg. Chem.*, 2008, **47**, 7813. b) N. N. Leyzerovich, K. G. Bramnik, T. Buhrmester, H. Ehrenberg, H. Fuess, *J. Power. Sources*, 2004, **127**, 76.

5 a) K. S. Park, S. D. Seo, H. W. Shim, D. W. Kim, *Nanoscale. Res. Lett.*, 2012, **7**. b) N. Sharma, K. M. Shaju, G. V. S. Rao, B. V. R. Chowdari, Z. L. Dong, T. J. White, *Chem. Mater.*, 2004, **16**, 504.

6 a) J. B. Zhou, N. Lin, L. B. Wang, K. L. Zhang, Y. C. Zhu, Y. T. Qian, *J. Mater. Chem. A*, 2015, **3**, 7463. b) Z. Y. Wang, S. Madhavi, X. W. Lou, *J. Phys. Chem. C*, 2012, **116**, 12508.

7 a) G. Y. Zhao, N. Q. Zhang, K. N. Sun, *J. Mater. Chem. A*, 2013, **1**, 221. b) Y. M. Sun , X. L. Hu, W. Luo, Y. H. Huang, *J. Mater. Chem.*, 2012, **22**, 425.

8 C. T. Cherian, M. V. Reddy, S. C. Haur, B. V. R. Chowdari, *Acs. Appl. Mater. Inter.*, 2013, **5**, 918.

9 B. Das, M. V. Reddy, S. Tripathy, B. V. R. Chowdari, *RSC. Adv.*, 2014, **4**, 33883.

10 J. Xia, L. X. Song, W. Liu, Y. Teng, Q. S. Wang, L. Zhao, M. M. Ruan, *RSC. Adv.*, 2015, **5**, 12015.

11 a) J. S. Xu, D. F. Xue, *J. Solid. State. Chem.*, 2007, **180**, 119. b) P. Liu, Y. Liang, X. Z. Lin, C. X. Wang, G. W. Yang, *ACS Nano*, 2011, **5**, 4748.

12 W. G. Chu, H. F. Wang, Y. J. Guo, L. N. Zhang, Z. H. Han, Q. Q. Li, S. S. Fan, *Inorg. Chem.*, 2009, **48**, 1243.

13 a) L. X. Song, J. Yang, L. Bai, F. Y. Du, J. Chen, M. Wang, *Inorg. Chem.*, 2011, **50**, 1682. b) L. X. Song, J. Xia, Z. Dang, J. Yang, L. B. Wang, J. Chen, *CrystEngComm*, 2012, **14**, 2675.

14 a) L. Yu, L. Zhang, H. B. Wu, G. Q. Zhang, X. W. Lou, *Energ. Environ. Sci.*, 2013, **6**, 2664. b) Z. C. Bai, N. Fan, C. H. Sun, Z. C. Ju, C. L. Guo, J. Yang, Y. T. Qian, *Nanoscale*, 2013, **5**, 2442.

15 a) U. K. Sen, S. Mitra, *RSC. Adv.*, 2012, **2**, 11123. b) M. Wang, G. D. Li, H. Y. Xu, Y. T. Qian, J. Yang, *ACS Appl. Mater. Interfaces*, 2013, **5**, 1003. c) P. Meduri, E. Clark, J. H. Kim, E. Dayalan, G.U. Sumanasekera, M. K. Sunkara, *Nano Lett.*, 2012, **12**, 1784..

16 Z. Xing, Z. C. Ju, J. Yang, H. Y. Xu, Y. T. Qian, *Electrochim. Acta*, 2013, **102**, 51.

17 a) S. J. Ding, D. Y. Zhang, J. S. Chen, X. W. Lou, *Nanoscale*, 2012, **4**, 95. b) C. Wang, W. Wan, Y. H. Huang, J. T. Chen, H. H. Zhou, X. X. Zhang, *Nanoscale*, 2014, **6**, 5351.

18 a) X. H. Huang, C. B. Wang, S. Y. Zhang, F. Zhou, *Electrochim. Acta*, 2011, **56**, 6752. b) F. Wang, W. Z. Tao, M. S. Zhao, M. W. Xu, S. C. Yang, Z. B. Sun, L. Q. Wang, X. P. Song, *J. Alloy. Compd.*, 2011, **509**, 9798.

19 a) W. J. Zhao, N. Du, H. Zhang, D. R. Yang, *J. Power. Sources*, 2015, **285**, 131. b) H. Wu, N. Du, J. Z. Wang, H. Zhang, D. R. Yang, *J. Power. Sources*, 2014, **246**, 198.

20 W. Xiao, J. S. Chen, C. M. Li, R. Xu, X. W. Lou, *Chem. Mater.*, 2010, **22**, 746.

21 a) G. Zhang, H. B. Wu, H. E. Hoster, X. W. Lou, *Energ. Environ. Sci.*, 2014, **7**, 302. b) L. Zhou, D. Zhao, X. W. Lou, *Adv. Mater.*, 2012, **24**, 745.

22 a) N. Du, Y. F. Xu, H. Zhang, J. X. Yu, C. X. Zhai, D. R. Yang, *Inorg Chem.*, 2011, **50**, 3320. b) J. Z. Wang, N. Du, H. Zhang, J. X. Yu, D. R. Yang, *J. Phys. Chem. C*, 2011, **115**, 23620.

23 a) X. L. Sun, C. L. Yan, Y. Chen, W. P. Si, J. W. Deng, S. Oswald, L. F. Liu, O. G. Schmidt, *Adv. Energ. Mater.*, 2014, **4**. b) X. Q. Liu, I. Willner, *Adv. Mater.*, 2013, **25**, 349.

24 Y. M. Sun, X. L. Hu, W. Luo, Y. H. Huang, *J. Mater. Chem.*, 2011, **21**, 17229.

25 a) B. Dasa, M. V. Reddya, C. Krishnamoorthia, S. Tripathyb, R. Mahendirana, G. V. Subba Raoa, B. V. R. Chowdaria, *Electrochim. Acta*, 2009, **54**, 3360. b) K. S. Park, S. D. Seo, H. W. Shim, D. W. Kim, *Nanoscale Res. Lett.*, 2012, **7**, 35.

26 S. Brunauer, P. H. Emmett, E. Teller, *J. Am. Chem. Soc.*, 1938, **60**, 309.

27 E. P. Barrett, L. G. Joyner, P. P. Halenda, *J. Am. Chem. Soc.*, 1951, **73**, 373.

28 a) J. T. Zai, K. X. Wang, Y. Z. Su, X. F. Qian, J. S. Chen, *J. Power Sources*, 2011, **196**, 3650. b) F. C. Zheng, D. Q. Zhu, Q. W. Chen, *ACS Appl. Mater. Interfaces*, 2014, **6**, 9256.

29 a) K. X. Wang, X. H. Li, J. S. Chen, *Adv. Mater.*, 2015, **27**, 527. b) S. K. Liu, Z. X. Chen, K. Xie, Y. J. Li, J. Xu, C. M. Zheng, *J. Mater. Chem. A*, 2014, **2**, 13942.

Graphical Abstract

Construction of $Cu_3Mo_2O_9$ Nanoplates with Excellent Lithium Storage Properties Based on a pH-Dependent Dimensional Change†

Juan Xia, Le Xin Song, Wei Liu, Yue Teng, Li Zhao, Qing Shan Wang and Mao Mao Ruan

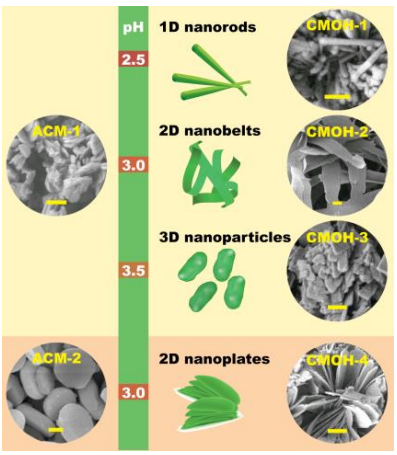

1D, 2D and 3D nanostructures of CMOHs were successfully constructed through a pH-dependent dimensional transformation of ACM.